EPJ Web of Conferences **355**, 04001 (2026) https://doi.org/10.1051/epjconf/202635504001
STAAAR 2025

Investigating the Impact of Geometric Variations on Vortex-Induced Performance of Bladeless Wind Turbines: A CFD Study

Atharv Kumar Pal[1], *Gershom* Thomas[1], *Rohit* Sharma[1*], and *Akhilesh* Sreehari[1]
[1]School of Mechanical Engineering, VIT Bhopal University, Sehore, Madhya Pradesh - 46614, India

Abstract. Bladeless wind turbines (BWTs) have gained attention for their low-cost, low-maintenance, and noise-free operation compared to conventional designs, yet their aerodynamic performance, particularly the influence of mast geometry on vortex-induced vibrations (VIV) and energy harvesting efficiency, remains insufficiently explored. While most studies focus on cylindrical masts, the role of non-circular cross-sections in urban low-speed flows is largely unaddressed. This study performs a comparative Computational Fluid Dynamics (CFD) analysis of four BWT mast geometries - two cylindrical (diameters 20 cm and 22.5 cm) and two elliptical (major/minor axes 22.5 × 11.25 cm and 25 × 12.5 cm) at wind speeds of 1, 3, and 5 m/s. Lift coefficient time histories and velocity curl contours reveal that cylindrical models produce strong, sustained periodic vortex shedding with high-amplitude oscillations, with the 22.5 cm cylinder (Model 2) exhibiting the most coherent and energetic response across all speeds, making it the most effective for VIV-based energy extraction. Elliptical models demonstrate superior aerodynamic damping; the smaller elliptical section (Model 3) achieves the strongest suppression of VIV, characterized by rapid transient decay, minimal wake vorticity, and low-amplitude oscillations, particularly at higher velocities. The larger elliptical model (Model 4) provides intermediate performance with more persistent but less intense shedding. These results highlight the critical impact of cross-sectional geometry on VIV characteristics and suggest that elliptical profiles, especially lower aspect ratios offer significant potential for vibration control, while larger cylindrical designs remain optimal for maximizing energy harvesting in small-scale urban BWT systems.

1 Introduction

The world is facing a major energy crisis, exacerbated by climate change and the rapid depletion of fossil fuels. In 2018, global energy consumption increased by 2.3 percent, accelerating the transition to renewable energy as a means to tackle these challenges. At current consumption levels, reserves of natural gas are expected to last another 37 years, of natural oil for 35 years, and of coal for around 107 years, implying that global fossil fuel supplies may be depleted within the century [1]. This scenario highlights the pressing need for efficient and sustainable energy solutions. Wind power has significant worldwide potential, especially onshore. The estimated technical onshore wind energy potential varies

* Corresponding author: rohit.sharma@vitbhopal.ac.in

© The Authors, published by EDP Sciences. This is an open access article distributed under the terms of the Creative Commons Attribution License 4.0 (https://creativecommons.org/licenses/by/4.0/).

from 20,000 to 50,000 TWh (terawatt-hours) per year, greatly exceeding the world's current total power consumption of around 15000 TWh [2].

Traditional wind turbines, despite their extensive use, encounter numerous limitations: diminished efficiency in areas with strong winds, substantial land requirements, elevated installation expenses, and significant mechanical maintenance costs. These limitations render them less appropriate for non-commercial, decentralized, or urban settings where alternatives that are low-maintenance, compact, and quieter are essential.

Bladeless wind turbines, also known as BWTs, offer a potential alternative for harnessing wind power by utilizing Vortex-induced vibration (VIV) to transform wind energy into mechanical energy instead of traditional rotating blades [3-4]. Despite their appeal due to minimal noise, slight motion, lower upkeep requirements, and compact size, they have not been extensively studied. There is a scarcity of thorough design validation data for the aerodynamics of BWT mast structures. Most of the research has concentrated on the basic principles of wave shedding and simplified models, rather than exploring how specific changes in geometry affect VIV efficiency.

In light of these gaps, the current research conducts an in-depth computational analysis of various BWT tower designs utilizing Computational Fluid Dynamics (CFD). The goal is to examine the impact of alterations in shape and size on vortex shedding, lift coefficient performance, and energy generation potential in urban wind environments. With a lack of reliable experimental data or accepted numerical benchmarks for BWTs, this study offers fresh CFD-driven perspectives that lay the groundwork for upcoming investigations and advancements. The results offer suggestions for enhancing compact BWT setups tailored for urban and distributed energy uses, especially in situations where conventional turbines are not feasible.

2 Literature review

2.1 Bladeless Wind Turbine

BWTs are an emerging technology with high potential in electricity generation via wind energy. Unlike traditional wind turbines that rely on propellers and specific wind speeds and directions to produce electricity, BWT generate power from low-speed winds coming from any direction, without the need for rotating blades. Figure 1 depicts a wind moving at free stream velocity encountering a cylindrical structure. The pressure differential created by flow separation causes alternating vortices to develop downstream of the cylinder, resulting in an oscillating wake pattern [5-6].

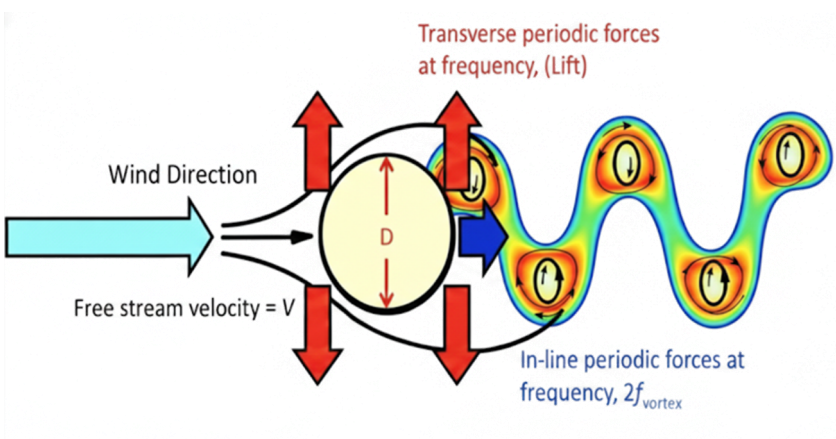

Fig. 1. The formation of vortices around the cylinder results in a periodic, oscillating wake pattern [6].

During the operation of a BWT system, the mast changes energy internally due to the wind's movement causing it to sway at its inherent frequency. This event, referred to as Von Kármán vortex shedding, happens when a material like air travels over the mast's exterior, causing vibrations [5].

When the wind hits the mast, it disrupts the movement, causing a turbulent fluid flow. This turbulence creates swirling patterns called vortices, which are spinning streams of fluid changing direction as they travel along the mast. These movements are known as VIV. These swirls trigger vibrations in the mast, generating back-and-forth motion that is converted into rotational power, ultimately producing electricity. BWTs can function efficiently in urban wind situations, making them adaptable for use in areas with irregular or low wind velocities [6].

2.2 Wind Condition in India

BWT provides several advantages which makes them a feasible alternative to traditional wind turbines, especially when it comes to noise reduction, maintenance, and efficiency in some situations. By harvesting electricity through VIV, BWT suffers low wear on machinery due to fewer moving parts, resulting in decreased maintenance costs and enhanced operational longevity. Additionally, BWTs are very suitable for some areas of India. The average wind speed in Tamil Nadu, Maharashtra, and Rajasthan has been reported to be between 3 and 8 m/s [7]. Coastal regions like Gujarat and Tamil Nadu have increased wind speeds because of the temperature difference between land and sea, creating sea breezes and local winds. Also, as shown in Figure 2, raising the hub height from 120 m to 150 m above ground level (AGL) substantially increases India's estimated onshore wind power potential, particularly in Maharashtra and Rajasthan, which become the dominant states at the higher height. This reflects the fact that wind speeds are higher and more consistent at elevated heights, making taller turbines more viable in these regions. Recent research suggests that cities offer significant opportunities for utilizing wind power, known as urban or micro wind farms. Areas like highways, tall building rooftops, railway paths, and gaps among multi-story buildings can be used efficiently for generating wind power. Nevertheless, understanding the disorderly and inconsistent wind patterns in urban areas is a major obstacle in this field. With proper attention, micro-wind farms could become a valuable additional method for producing energy, supporting conventional wind farms [8].

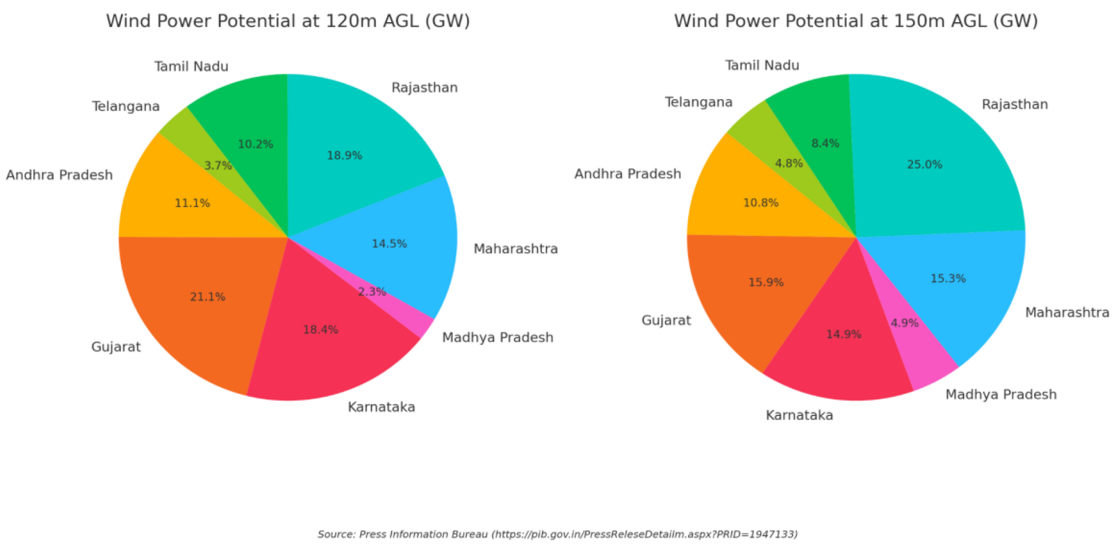

Fig. 2. State-wise onshore wind power potential in India at 120 m and 150 m hub heights (AGL).

3. Numerical Setup

3.1 Computational Domain and Geometry Simplification

The symmetrical flow's properties are utilized by using a two-dimensional (2D) model to reduce the processing needs. This approach significantly lowers computational costs while capturing important features of the flow, such as vortex shedding. The computational area is given as 500 cm long and 100 cm wide, with each bluff body's midpoint positioned 40 cm from the intake. The left edge functions as the velocity inlet, and the right side is considered a pressure outlet. The upper and lower limits act as fixed walls, mimicking enclosed flow conditions. The structure is crafted using the Design Modeler within ANSYS, and meshing is executed using a mesh that mostly consists of quadrilaterals to ensure computational precision, incorporating local refinement near curvature.

3.2 Equation for Mass Conservation

The conservation of mass ensures that the mass entering a control volume equals the mass leaving it, assuming steady and incompressible flow. In Cartesian coordinates, the continuity equation is expressed as:

$$\frac{\partial \rho}{\partial t} + \frac{\partial \rho u}{\partial x} + \frac{\partial \rho v}{\partial y} + \frac{\partial \rho w}{\partial z} = 0 \tag{1}$$

The general vector form of the above equation is written as:

$$\frac{\partial \rho}{\partial t} + \nabla \cdot (\rho \bar{V}) = 0 \tag{2}$$

where, ρ denotes the fluid density, $\bar{V}$ is the velocity vector, v, and w are the velocity components in the x, y, and z directions respectively. $\nabla \cdot (\rho \bar{V})$ divergence of mass flux, indicating how mass flows into or out of a point.

3.3 Equation for Momentum Conservation

The momentum conservation equation governs the motion of fluid particles under the influence of various forces. It is derived from Newton's second law, which states that the rate of change of momentum of a fluid element equals the sum of the external forces acting upon it.

$$\rho \left(\frac{\partial \bar{V}}{\partial t} + \bar{V} \cdot \nabla \bar{V} \right) = -\nabla p + \mu \nabla^2 \bar{V} + \frac{1}{3} \mu \nabla (\nabla \cdot \bar{V}) + \overline{F_b} \tag{3}$$

where the left-hand side, $\rho \left(\frac{\partial \bar{V}}{\partial t} + \bar{V} \cdot \nabla \bar{V} \right)$, represents the total acceleration of the fluid both local (with time) and convective (with space). On the right-hand side, $-\nabla p$ accounts for pressure forces driving the flow, while $\mu \nabla^2 \bar{V}$ represents viscous effects that resist motion. The term $\frac{1}{3} \mu \nabla (\nabla \cdot \bar{V})$ appears in compressible flows to capture bulk viscosity. Lastly, $\overline{F_b}$ stands for external body forces like gravity.

3.4 Transport Equations for k-epsilon turbulence model

The model uses the realizable k-epsilon turbulence model to predict flow patterns with precision. A linked pressure–velocity method was used to boost computational stability, and all fundamental equations were tackled with a second-order implicit approach to enhance accuracy in time and space. The dynamic study spanned 300 time intervals of 0.01 seconds each, ensuring detailed temporal resolution of vortex shedding movements. To ensure convergence and accurately depict the flow's unsteady nature, a maximum of 20 iterations were permitted for each time step.

The underlying transport equations for k:

$$\frac{\partial}{\partial t}(\rho k) + \frac{\partial}{\partial x_j}(\rho k u_j) = \frac{\partial}{\partial x_j}\left[\left(\mu + \frac{\mu_t}{\sigma_k}\right)\frac{\partial k}{\partial x_j}\right] + M_k + M_b - \rho\epsilon - Y_N + S_k \tag{4}$$

The transport equations for epsilon (ϵ):

$$\frac{\partial}{\partial t}(\rho \epsilon) + \frac{\partial}{\partial x_j}(\rho \epsilon u_j) = \frac{\partial}{\partial x_j}\left[\left(\mu + \frac{\mu_t}{\sigma_\epsilon}\right)\frac{\partial \epsilon}{\partial x_j}\right] + \rho C_1 S\epsilon - \rho D_2 \frac{\epsilon^2}{k+\sqrt{\nu\epsilon}} + D_{1\epsilon}\frac{\epsilon}{k}D_{3\epsilon}M_b + S_\epsilon \tag{5}$$

where,

$$C_1 = \max\left[0.43, \frac{\eta}{\eta+5}\right], \eta = S\frac{k}{\epsilon}, S = \sqrt{2S_{ij}S_{ij}} \tag{6}$$

The terms M_k and represent the kinetic energy generated by mean velocity gradients and buoyancy forces, respectively, while Y_N accounts for the effects of fluctuating dilations. The constants $D_{1\epsilon}$ and D_2 are specific to the model, and S_k and S_ϵ are defined source terms. Additionally, σ_ϵ and σ_k are Prandtl numbers associated with the respective transport equations.

A transient analysis is conducted to capture the formation of von Kármán vortex streets, which are inherently time-dependent phenomena. Air is used as the working fluid, characterized by a density of 1.225 kg/m³ and a viscosity of 1.7894×10^{-5} kg/m·s. To assess model performance under different wind conditions, inlet velocities of 1 m/s, 3 m/s, and 5 m/s are applied.

3.5 Bladeless Wind Turbine Modelling

To assess the impact of mast geometry on aerodynamic efficiency and vortex generation, various mast configurations were analyzed. The chosen mast dimensions align with the size range typically found in existing small-scale bladeless wind turbine prototypes, where diameters generally range from 0.10 m to 0.30 m. This research focuses on non-commercial, urban micro-wind applications, such as installations on rooftops and building edges, emphasizing compact designs to ensure safety, ease of installation, and effective performance in low urban wind conditions. Besides cylindrical models, two elliptical designs were included to explore how differences in bluffness and aspect ratio affect vortex shedding, a relatively unexplored area in the context of BWTs. By keeping the frontal dimensions similar across all models, the study isolates the effects of geometry while adhering to established bluff-body aerodynamics principles. The geometry of the four distinct models examined in this study is described below:

1. Model 1 (M1) — a simple cylindrical structure with a diameter of 20 cm.
2. Model 2 (M2) — a slightly larger cylindrical structure with a diameter of 22.5 cm.
3. Model 3 (M3) — an elliptical design with a major axis of 22.5 cm and a minor axis of 11.25 cm.
4. Model 4 (M4) — a larger elliptical configuration with a major axis of 25 cm and a minor axis of 12.5 cm.

4. Results and Discussion

In this study, a comparative analysis of theoretical and simulated vortex-shedding frequencies was conducted for four bladeless wind turbine (BWT) mast geometries at wind speeds of 1 m/s, 3 m/s, and 5 m/s. The primary goal was to evaluate the influence of cross-sectional shape (cylindrical vs. elliptical) on vortex-shedding characteristics and its implications for energy-harvesting efficiency through vortex-induced vibrations (VIV).The performance of the models was assessed by comparing the theoretical frequencies, calculated using the Strouhal number (St = fL/U. where f = Oscillation frequency (vortex shedding frequency), L = Characteristic length, U = flow velocity (free stream velocity)), with the frequencies observed through simulation. The results presented in Table 1 provide insight into the response of different structural designs - cylindrical and elliptical shapes under varying wind speeds.

Table 1. The table compares the theoretical vortex-shedding frequencies with the simulated frequencies obtained from CFD for Model 1 and Model 2 at three different wind velocities: 1 m/s, 3 m/s, and 5 m/s.

Model	Wind Speed (m/s)	Theoretical Frequency (Hz)	Simulated Frequency (Hz)
M1	1	1.15	1.33
M1	3	3.45	4.98
M1	5	5.75	8.19
M2	1	1.02	1.66
M2	3	3.07	5.32
M2	5	5.11	8.31
M3	1	0.88	2.66
M3	3	2.66	9.38
M3	5	4.44	0.332
M4	1	1.6	2.31
M4	3	4.8	8.32
M4	5	8	12.9

Vortex-shedding frequency increases linearly with wind velocity for all four models in both simulated (CFD) and theoretical calculations as shown in the Figure 3. Geometry significantly influences the shedding frequency: larger models (M2 and M4) generally produce higher frequencies at higher speeds, while the smaller elliptical model (M3) shows relatively lower frequency response.

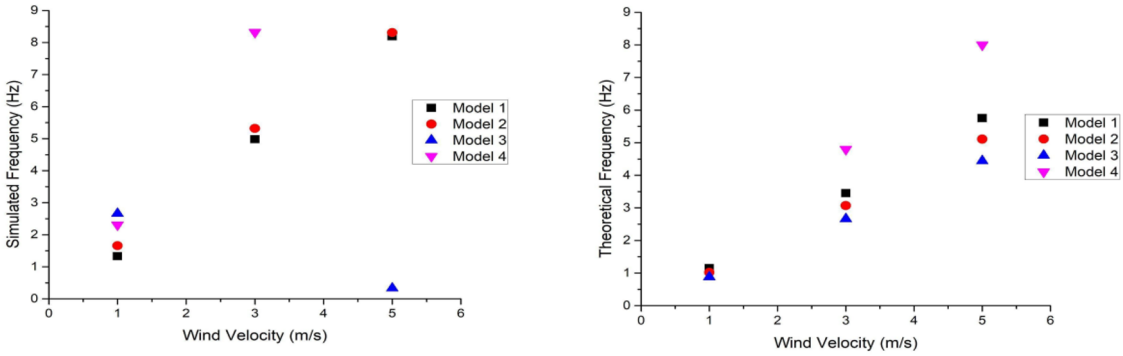

Fig. 3. Comparison of simulated and theoretical vortex-shedding frequencies for Models 1–4 at wind velocities of 1, 3, and 5 m/s. The left graph shows CFD-predicted frequencies derived from lift coefficient oscillations, while the right graph presents theoretical frequencies based on the Strouhal relationship.

Figure 4 shows four time-history graphs of the lift coefficient (Cl) for four distinct models (M1, M2, M3, and M4) with a constant wind speed of 5 m/s. Each subplot depicts the temporal evolution of Cl throughout a flow duration of 0–3 seconds. All models exhibit substantial, periodic vortex shedding. Cylindrical models (M1 and M2) show prolonged, high-amplitude oscillations. Elliptical models exhibit opposing behavior: M3 has extremely low-amplitude damped oscillations (high aerodynamic damping), but M4 sustains sustained periodic oscillations with lower damping than M3. Figure 5 shows the time history of lift coefficient (Cl) for models M1, M2, M3, and M4 at wind speed 3 m/s. Periodic oscillations are evident, with M1 and M2 exhibiting distinct fluctuations, M3 demonstrating a damped low-amplitude response, and M4 exhibiting more oscillatory persistence than M3. Figure 6 shows the time history of lift coefficient (Cl) for models M1, M2, M3, and M4 at wind speed 1 m/s. Low-frequency oscillations are observed, with M1 and M2 showing gradual amplitude growth, M3 displaying mild damped response, and M4 exhibiting slightly more pronounced low-amplitude fluctuations than M3.

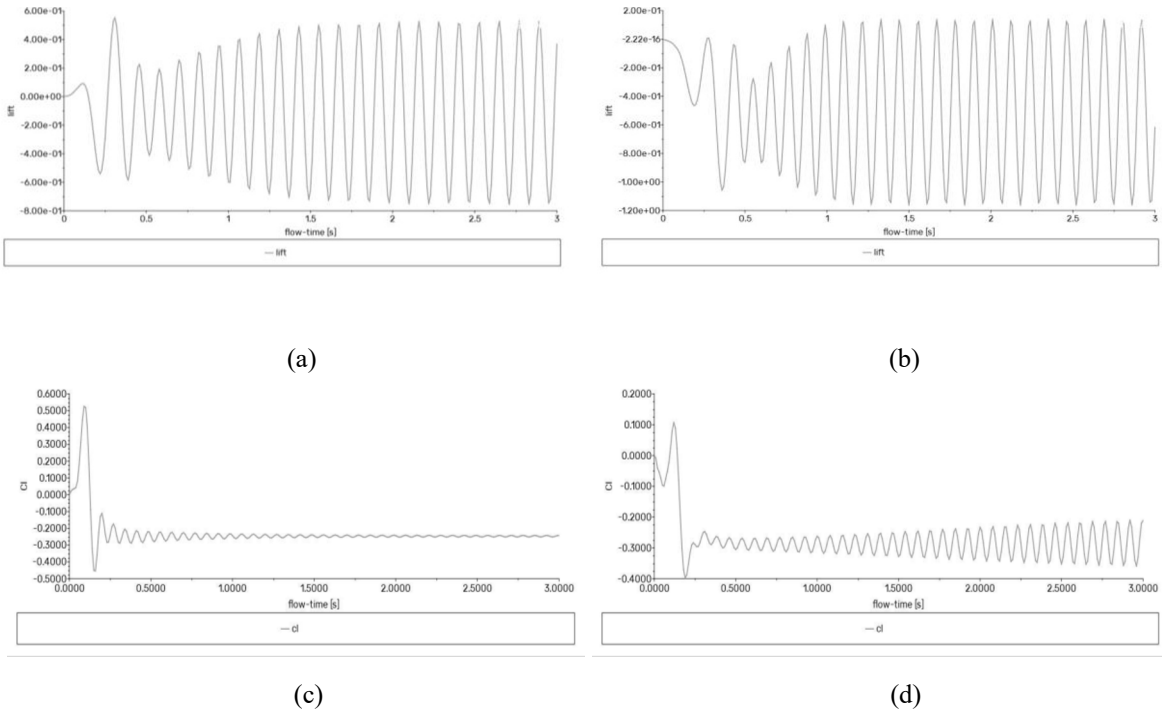

Fig. 4. Time history of lift coefficient (Cl) for models (a) M1, (b) M2, (c) M3, and (d) M4 at wind speed 5 m/s.

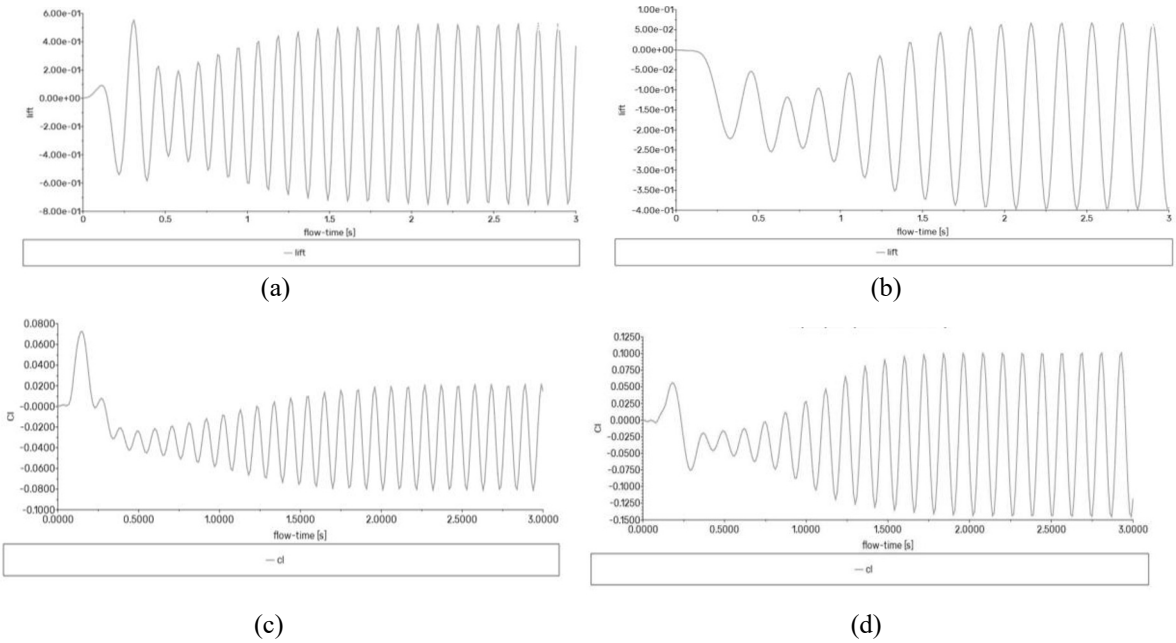

Fig. 5. Time history of lift coefficient (Cl) for models (a) M1, (b) M2, (c) M3, and (d) M4 at wind speed 3 m/s.

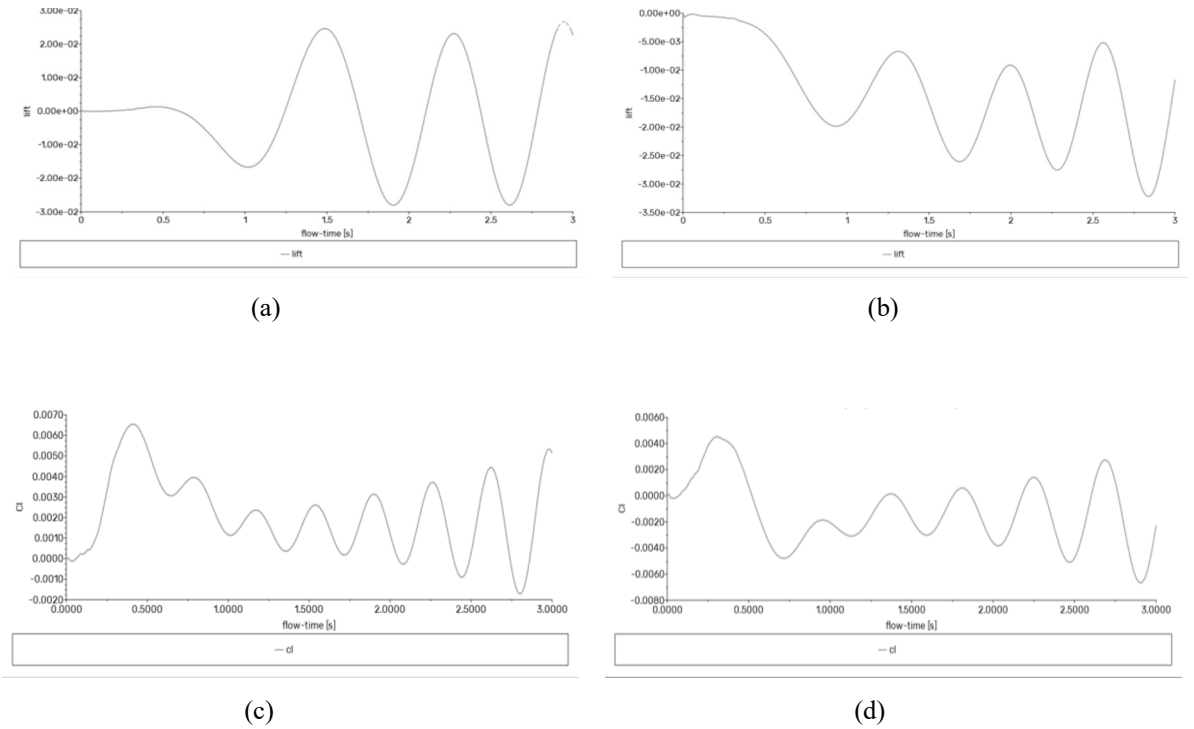

Fig. 6. Time history of lift coefficient (Cl) for models (a) M1, (b) M2, (c) M3, and (d) M4 at wind speed 1 m/s.

Velocity curl contours demonstrate distinct vortex-induced responses across the four models at wind speeds of 1 m/s, 3 m/s, and 5 m/s, as illustrated in Figure 7-9. At 5 m/s, cylindrical models (M1 and M2) exhibit strong, sustained periodic vortex shedding with high-amplitude lift oscillations (Figure 4a & 4b), accompanied by well-defined alternating vortex streets in the wake (Figure 7a & 7b). In contrast, the elliptical models display geometry-dependent damping: M3 shows rapid decay of initial transients, resulting in very low-amplitude damped oscillations (strongest aerodynamic damping), and a highly streamlined wake with minimal vorticity (Figure 7c). M4 maintains sustained periodic lift oscillations with moderate wake energy and less pronounced damping relative to M3 (Figure 4c, Figure 7c). At 3 m/s, vortex shedding weakens overall. Cylindrical models retain clear but reduced-intensity vortex streets (Figure 8a & 8b), while M3 produces a long, narrow wake with significantly lower vorticity, indicating superior flow alignment and damping (Figure 8c). M4 exhibits continuous shedding with alternating structures extending farther downstream than M3 as shown in Figure 8d.

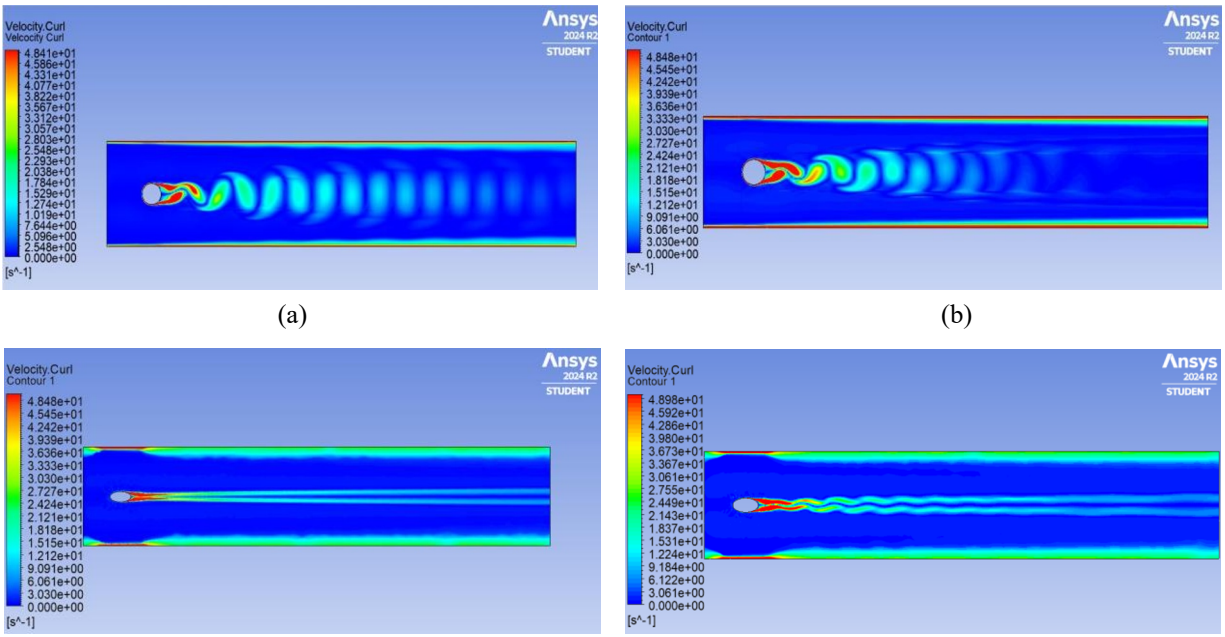

Fig. 7. Velocity curl contours of models (a) M1, (b) M2, (c) M3, and (d) M4 at wind speed 5 m/s.

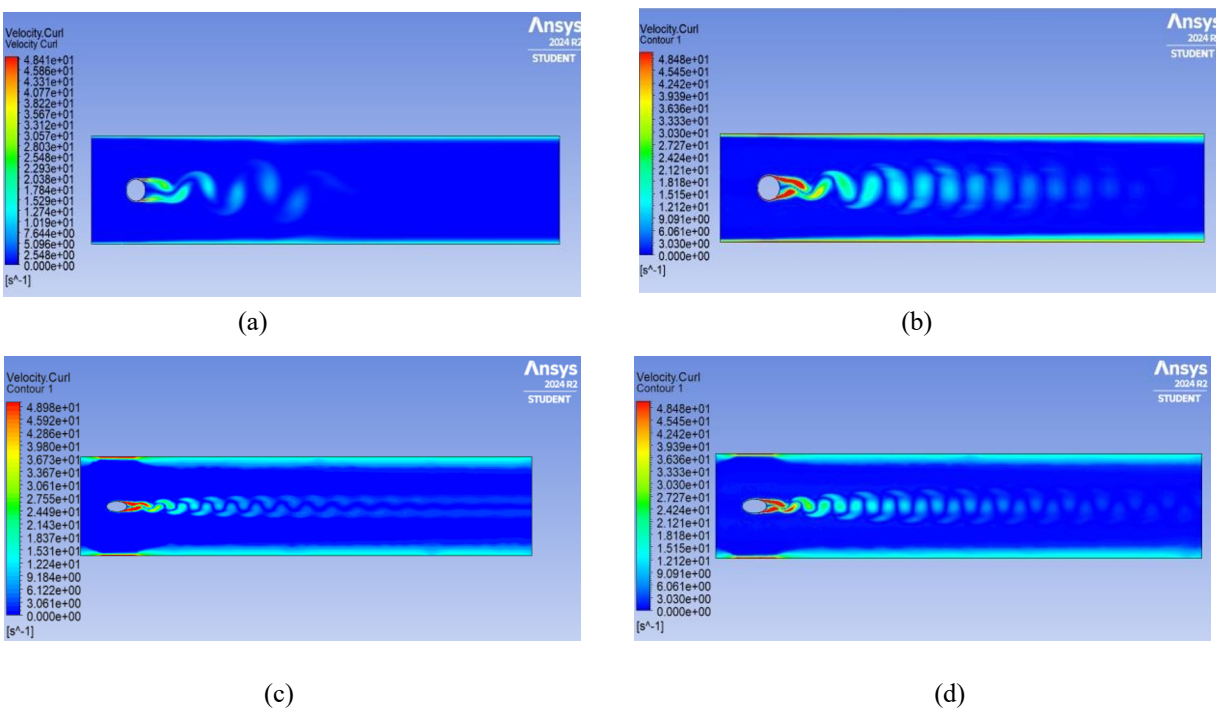

Fig. 8. Velocity curl contours of models (a) M1, (b) M2, (c) M3, and (d) M4 at wind speed 3 m/s.

At 1 m/s, wake structures are weak and less organized. M1 and M2 form short, low-intensity wakes with early-stage shedding (Figure 9a & 9b). M3 generates the narrowest wake with minimal vortex formation (Figure 9c), demonstrating the highest degree of streamlining. M4 displays a more energetic wake with periodic vortices persisting farther downstream than M3.

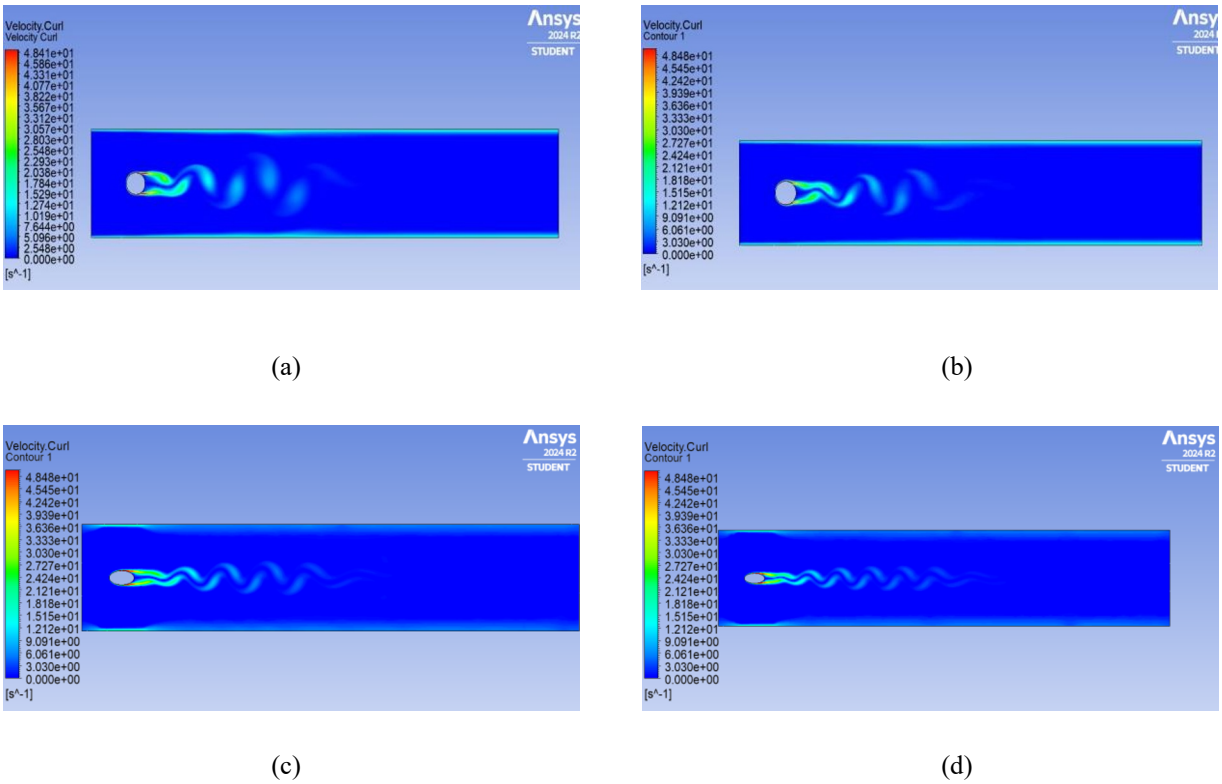

Fig. 9. Velocity curl contours of models (a) M1, (b) M2, (c) M3, and (d) M4 at wind speed 1 m/s.

5. Conclusion

The comparative CFD analysis of four mast geometries for bladeless wind turbines under low urban wind speeds (1–5 m/s) demonstrates that cross-sectional shape has a significant influence on vortex-induced vibration characteristics and energy harvesting potential. Cylindrical masts generate strong, coherent vortex shedding with high-amplitude lift oscillations, with the larger cylinder (Model 2, 22.5 cm diameter) exhibiting the most energetic and steady response across all speeds - making it the optimal configuration for maximizing VIV-based power extraction. In contrast, elliptical masts provide superior aerodynamic damping: the smaller elliptical section (Model 3) has the strongest suppression of vortex formation, rapid transient decay, minimal wake vorticity, and lowest oscillation amplitudes, particularly at higher velocities, positioning it as the preferred geometry for vibration-sensitive applications requiring structural stability. The larger elliptical mast (Model 4) provides intermediate performance with more consistent but moderated shedding.

These findings fill a key gap in our understanding of non-circular mast aerodynamics and provide actionable insights for BWT design: cylindrical profiles for enhanced energy yield in controlled environments, and elliptical (especially lower aspect ratio) profiles for robust vibration mitigation in urban settings prone to variable gusts. Future research should focus on experimental validation, higher Reynolds number regimes, and multi-objective optimization to balance energy output with structural lifespan in real-world deployments.

Acknowledgements

The authors extend their sincere gratitude to VIT Bhopal University for providing essential support for the simulation work. Grok AI tool was used for language refinement and improving the clarity of the manuscript. All technical content, results, and conclusions are the sole work of the authors.

References

1. Shafiee, S. & Topal, E. When will fossil fuel reserves be diminished? *Energy Policy* **37**, 181–189 (2009).
2. Sholapurkar, R. B. & Mahajan, Y. S. Review of wind energy development and policy in India. *Energy Technol. & Policy* **2**, 122–132 (2015).
3. Elsayed, A. M. & Farghaly, M. B. Theoretical and numerical analysis of vortex bladeless wind turbines. *Wind Eng.* **46**, 1408–1426 (2022).
4. Das, A., Rahimi, M. & others. Effects of Geometry in 2D Simulations for Vortex-Induced Vibration of Bladeless Wind Turbines. *Iran. J. Chem. Chem. Eng.* **44**, 203–215 (2025).
5. White, F. M. Fluid Mechanics 7th Edition in SI units. at (2016).
6. Ramadhany, M. F., Kusuma, T. A., Chelsie, Y. N. & Adi, G. S. Optimization of Mechanical Design Bladeless Wind Turbine for Electricity Fulfilment in Nusa Tenggara Timur, Indonesia. *arXiv Prepr. arXiv2205.02786* (2022).
7. Satyanarayana Swamy, P. V. V, Ramachandra Murthy, K. V. S. & others. Research into wind speeds and energy generation in India: an overview. *Recent Dev. Electron. Commun. Syst.* 31–37 (2023).
8. Tasneem, Z. *et al.* An analytical review on the evaluation of wind resource and wind turbine for urban application: Prospect and challenges. *Dev. Built Environ.* **4**, 100033 (2020).